Chem Comm

RSCPublishing

COMMUNICATION

Selective sensing of 2,4,6-trinitrophenol (TNP) in aqueous media with "aggregation-induced emission enhancement" (AIEE)-active iridium(III) complexes

Cite this: DOI: 10.1039/xoxxoooooox

Received ooth January 2012,
Accepted ooth January 2012

DOI: 10.1039/xoxxoooooox

www.rsc.org/

Weilong Che,[a] Guangfu Li,[a] Xingman Liu,[a] Kuizhan Shao,[a] Dongxia Zhu,*[a] Zhongmin Su*[a] and Martin R. Bryce*[b]

A series of new phosphorescent cyclometalated iridium(III) complexes which possess aggregation-induced emission enhancement (AIEE) detect 2,4,6-trinitrophenol (TNP) selectively with high quenching constants in aqueous media. The sensing mechanism was systematically investigated by mass spectrometry, ^{1}H and ^{19}F NMR spectroscopy. X-ray crystal structure analysis reveals an O-H···O interaction between TNP and the ancillary ligand which explains the high selectivity for TNP compared to other nitro-aromatics.

Nitro-aromatics such as 2-nitrotoluene (oNT), nitrobenzene (NB), 2,4,6-trinitrotoluene (TNT) and 2,4,6-trinitrophenol (TNP) (picric acid) are widespread explosive materials that threaten society through terrorist activities. TNP exhibits enhanced explosive power compared to TNT.[1] TNP is also a notorious environmental pollutant of irrigation land and ground water supplies due to its high acidity and good solubility in water.[2] The selective detection of TNP from mixtures of other nitro-aromatic explosives is very difficult because they all exhibit strong electron affinity.[3] Therefore, there is an urgent need for an efficient selective sensor for detecting TNP.[4] The current detection methods for organic analytes include Raman spectroscopy, cyclic voltammetry, gas chromatography, mass spectrometry, ion mobility spectrometry, electrochemical sensing, photoluminescence (PL) spectroscopy and others.[5] Among these reported methods, PL-based methods have received significant attention due to their relative simplicity, rapid response time, high selectivity, high sensitivity and low cost.[6]

A variety of PL materials including dual-emission quantum dot hybrids,[7] microporous metal-organic frameworks (MOFs),[8] conjugated polymers (CPs)[9] and fluorescent film sensors,[10] have been used to detect of nitro-aromatics. A drawback of this strategy is that due to aggregation-caused quenching (ACQ) the emission intensity decreases when the concentration of the luminophores increases.[11] However, Tang's group pioneered a class of compounds which show almost no luminescence in solution and a dramatic enhancement of emission in the aggregated state, named aggregation-induced emission (AIE).[12] The similar phenomenon of AIE enhancement (AIEE) was subsequently reported by Park et al.[13] Fluorescence-based sensors often suffer from small Stokes shifts and photobleaching effects.[14] On this account, the development of phosphorescent iridium(III) complexes as chemosensors represents a breakthrough.[15] This is because of the excellent photophysical properties of Ir(III) complexes such as long emissive lifetimes, large Stokes shifts, high quantum yields, and easy tuning of emission wavelength compared to the fluorescent analogues.[16] Furthermore, most Ir(III) complexes are thermally and chemically stable and are strongly emissive at room temperature. Ir(III) complexes have high sensitivity and selectivity for the detection of nitro-aromatic explosives and have relatively low detection limits compared to reported fluorescent AIE materials.[17] Thus, by combining the desirable features of AIE and phosphorescence, the development of new AIE- or AIEE-active Ir(III)-based sensors is a promising solution for contemporary challenges for today's society.[18]

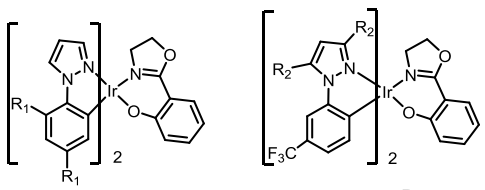

	R_1		R_2
Complex 1	F	**Complex 3**	H
Complex 2	Cl	**Complex 4**	CH_3

Fig. 1 Chemical structures of the complexes **1**-**4**.

AIE occurs due to the restriction of intramolecular motions (RIM) in the aggregated state, thereby blocking the nonradiative pathways and opening up a radiative channel.[19] We have previously reported an iridium complex ($(ppy)_2Ir(oz)$) with 2-(2'-hydroxyphenyl)-2-oxazoline (Hoz) as an ancillary ligand, shown in Fig. S1a (ESI†).[20] The crystal packing of $(ppy)_2Ir(oz)$ has relatively weak C-H···π (2.77-2.86 Å) intermolecular interactions which result in an effective pathway for nonradiative decay in the crystalline state (Fig. S1b, ESI†) and $(ppy)_2Ir(oz)$ shows strong ACQ (Fig. S5, ESI†). We reasoned that the introduction of electron-withdrawing substituents, such as fluorine, chlorine or a trifluoromethyl group, into the cyclometalated ligands should enhance intermolecular interactions and thereby restrict the molecular motions in the aggregated state and hence allow AIE to occur, instead of ACQ.

Up to now, there are very few studies on the detection of explosives with AIE-active Ir(III) complexes.[21] Laskar et al. reported that two Ir(III) complexes detect TNP by a mechanism which combines electron and energy transfer.[22] Mukherjee et al. observed that the high acidity of TNP[23] caused luminescent MOFs to decompose, making detection of TNP unreliable, whereas other nitro-aromatics were successfully sensed by MOFs.[24]

We now report that the strongly acidic TNP interacts with the new Ir(III) complexes **1-4** (Fig. 1) and effectively inhibits their AIEE properties. This leads to the desired highly selective and sensitive phosphorescent detection of TNP in aqueous media.

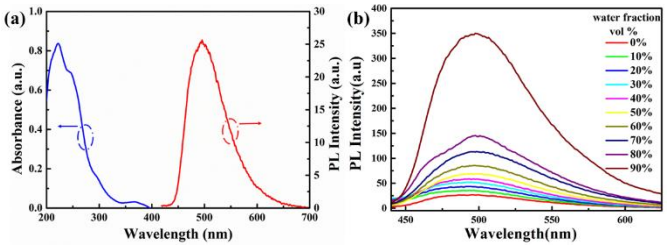

Fig. 2 (a) UV-Vis absorption and emission spectra of complex **1** (10 μM) in acetonitrile solution at room temperature. (b) Emission spectra of complex **1** (10 μM) in acetonitrile-water mixtures with different water fractions (0-90% v/v) at room temperature.

Complexes **1-4** possess good solubility in acetonitrile, and the solutions are weakly emissive. A gradual enhancement of PL intensity is observed with increasing the water fraction in the acetonitrile-water mixture, indicating that complex **1** is AIEE active (Fig. 2). Transmission electron microscopy and electron diffraction experiments indicated that crystalline aggregates are formed in the mixtures with a water ratio of 90% (Fig. S6, ESI†). The phosphorescent quantum yield of complex **1** in the solid state is 30% and this relatively strong emission can be attributed to the presence of the fluorine atoms, as the comparable value for the non-fluorinated analogue is only 4%. The packing in the X-ray crystal structure of **1** shows several short C-H···F intermolecular interactions with distances of 2.49-2.50 Å (Fig. 3). These contacts can effectively restrict the intramolecular motion of complex **1**, thus blocking the nonradiative pathways in the solid state. The complexes **2-4** also show an AIEE effect (Fig. S7-S9, ESI†) and they exhibit short intermolecular contacts, which are π···π (complex **2**) or C-H···F (complexes **3-4**) with distances of 3.55 Å (π···π) or 2.74 Å (C-H···F) or 2.55-2.79 Å (C-H···F) in the crystalline state (Fig. S2-S4, ESI†). These interactions could also limit intramolecular motions. The phosphorescence quantum yields of **2-4** in the solid state are 18%, 14% and 8%, respectively.

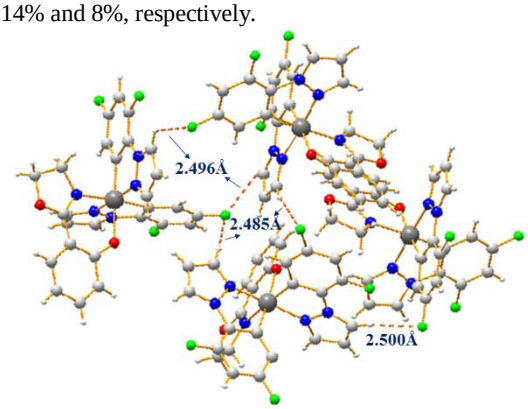

Fig. 3 Molecular packing of complex **1** in the crystal with short intermolecular contacts shown as dashed lines.

Complexes **1-4** effectively prevent emission quenching in aqueous media by virtue of their AIEE properties. The phosphorescence quantum yields of **1-4** in acetonitrile-water (1:9 v/v) solution are 21%, 15%, 11% and 10%, respectively. Therefore, TNP detection was investigated. As shown in Fig. 4a, complex **1** displays strong phosphorescence at around 500 nm in acetonitrile-water (1:9 v/v) (10 μM) solution without TNP, and a rapid quenching of emission is visible when the concentration of TNP is increased. The quenching is clearly identified when 0.5 ppm of TNP is added and 99% of the emission is quenched when the TNP concentration reached 5 ppm. Similarly, the phosphorescence of complexes **2-4** is also quenched by TNP in acetonitrile-water (1:9 v/v) (10 μM) solutions, with quenching efficiencies of 95%, 97% and 94%, respectively (Fig. S10-S12, ESI†). The emission of **1-4** is immediately quenched when TNP is added to the solutions, indicating that TNP rapidly interacts with the complexes. This facilitates the effective "real-time" detection of TNP.

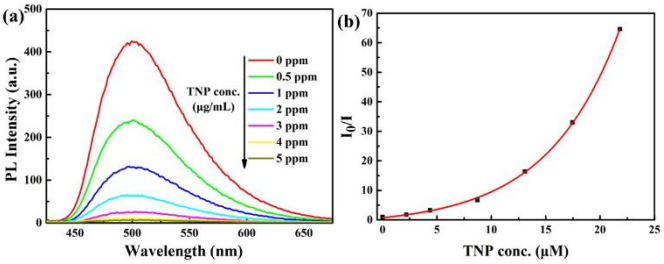

Fig. 4 (a) PL spectra of complex **1** (10 μM) in acetonitrile-water (v/v = 1:9) containing different amounts of TNP. (b) Corresponding Stern-Volmer plot of TNP.

The Stern-Volmer (S-V) plot for complex **1** is nonlinear and shows that higher concentrations of TNP lead to a higher efficiency of emission quenching (Fig. 4b). The quenching constant is 1.50×10^5 M^{-1} for complex **1**, which is relatively high compared to the reported Ir(III) complexes.[21a, 22, 25] The S-V curves for complexes **2-4** are also nonlinear, and the quenching constants are 0.32×10^5 M^{-1}, 1.66×10^5 M^{-1} and 0.86×10^5 M^{-1}, respectively (Fig. S10-S12 and discussion in ESI†). The detection limits for complexes **1-4** as sensors for TNP are calculated to be 0.23, 0.15, 1.05 and 1.65 μM, respectively.[26]

The emission response of complex **1** to different nitro-aromatic explosives, namely 2,4,6-trinitrotoluene (TNT), 3-nitrotoluene (mNT), nitrobenzene (NB), 2,6-dinitrotoluene (2,6-DNT), 2,4-dinitrotoluene (2,4-DNT), 2-nitrotoluene (oNT) and 1,3-dinitrobenzene (1,3-DNB), established high selectivity for TNP (Fig. 5a). Compared with TNP, other nitro-aromatics have little effect under the same conditions. In addition, the response of different concentrations of nitro-aromatics to the emission quenching of complex **1** was also evaluated (Fig. S13, ESI†). It is observed that with the increase in concentration of the nitro-aromatic species, TNP clearly enhances the quenching efficiency, whereas the others showed no distinct change. It is worth noting that the emission intensity is significantly quenched after the addition of TNP (5 ppm) into the systems containing other nitro-aromatics (Fig. 5b), indicating that the other compounds have little effect on the detection of TNP by complex **1**. These results demonstrate the excellent selectivity of complex **1** for TNP. Considering the strong acidity of TNP, we also investigated the response of complex **1** to TNP in CH_3CN/aqueous HEPES buffer (1 mM, pH 7.3; 1:4, v/v) solution (Fig. S14, ESI†). The data show that complex **1** has relatively good sensitivity and selectivity for the detection of TNP, indicating that TNP interacts with complex **1** even in HEPES buffer solution. As depicted in Fig. S15-S17, similar phenomena are also

observed with complexes **2-4**, which are also suitable for selective detection of TNP.

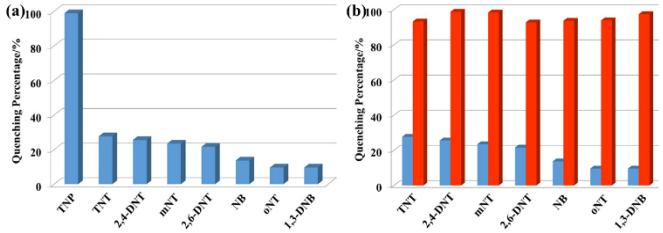

Fig. 5 (a) Quenching percentage obtained for different analytes (5 ppm). (b) Quenching percentage of complex **1** (10 μM) with analytes (5 ppm) in acetonitrile-water (v/v = 1:9) mixtures before (blue) and after (red) the addition of 5 ppm TNP.

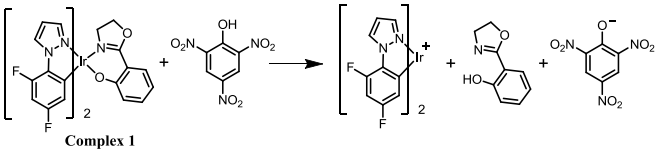

Scheme 1 A proposed mechanism for the reaction of complex **1** with TNP.

The origin of the selectivity of complexes **1-4** towards TNP was investigated and the proposed mechanism is shown for complex **1** in Scheme 1. Spectroscopic evidence to support this mechanism is presented in the ESI. To probe the interaction between complex **1** and TNP, a single crystal of **1·TNP** suitable for X-ray analysis was obtained. An O-H···O interaction between complex **1** and TNP was clearly observed, and the Ir-O bond lengthened from 2.11 Å in **1** to 2.20 Å in **1·TNP** (Fig. 6). This suggests that a specific binding of TNP initiates the fragmentation of complex **1** that is observed spectroscopically, as discussed in the ESI. The proton of TNP will dissociate more easily in acetonitrile-water medium than in dichloromethane solution used for growing the crystals. We conclude, therefore, that a specific O-H···O interaction between TNP and the complexes **1-4** plays a significant role in the sensing system. Under the same conditions, the emission intensities of complexes **1-4** after addition of 5 ppm of 2,4-dinitrophenol (2,4-DNP) are quenched much less compared to TNP (Fig. S27, ESI†). This is due to the increased acidity of 2,4-DNP (pKa = 4.11) and TNP (pKa = 0.38) in aqueous media.[27] This accounts for the selective detection of TNP.

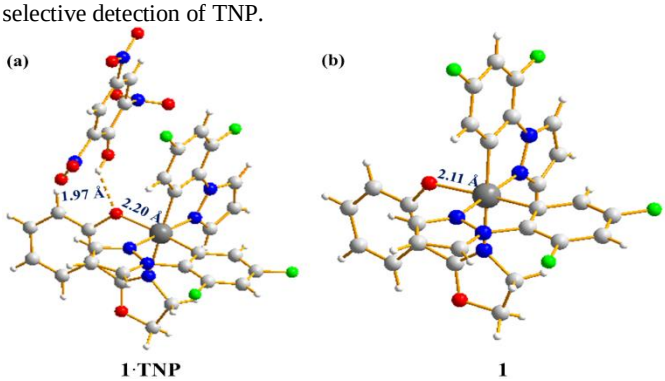

Fig. 6 Crystal structure of complex **1·TNP** (a) and complex **1** (b). Both single crystals were obtained by slow evaporation of dichloromethane.

Other nitro-aromatic compounds weakly decrease the emission intensity of **1-4**. This may be due to the fact that the nitro compounds are electron deficient, and if the lowest unoccupied molecular orbital (LUMO) energies of the complexes are higher than those of the analytes, then photoinduced electron transfer (PET) can occur from complexes to analytes, leading to the emission intensity decrease.[21a]

To confirm this hypothesis, the structures of complexes **1-4** were optimized by referring to the X-ray diffraction data, and their highest occupied molecular orbital (HOMO) and LUMO energy levels in solution were calculated by DFT methods. The higher energy LUMOs of the complexes facilitate the transfer of electrons to the lower LUMOs of the nitro-aromatics, establishing that PET is a lausible mechanism for slightly decreasing the complexes' emission in response to a range of nitro-aromatic compounds (Fig. S28, ESI†). The PET process may also occur between TNP and the complexes **1-4**, but TNP also leads to the decomplexation of the Hoz ligand in aqueous media; and this is the main mechanism for the highly selective sensing of TNP.

To demonstrate a practical application of complex **1** as a sensor for TNP, filter papers that emit strong phosphorescence under 365 nm UV illumination were prepared by their immersion in an acetonitrile solution of complex **1** and then drying at room temperature in air. It can be seen clearly with the naked eye that the phosphorescent paper was stained by adding a drop of a solution of TNP (5 ppm) in acetonitrile-water (1:9 v/v) (Fig. 7). For control experiments, adding solutions of other nitro-aromatic compounds onto the phosphorescent papers led to no obvious change. These results clearly illustrate that complex **1** is suitable for immediate visualization of traces of TNP by a very simple practical method that should be applicable for rapid on-site testing.

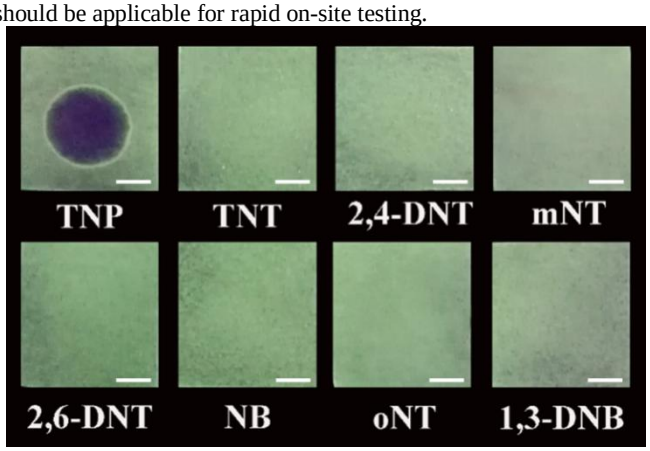

Fig. 7 Luminescent photographs of filter papers impregnated with complex **1** against 5 ppm of different nitro-aromatic compounds. All photographs were taken under 365 nm UV illumination. The scale bar is 5 mm.

In conclusion, four new AIEE-active iridium(III) complexes detect TNP selectively over a range of other nitro-aromatic compounds with high efficiency in aqueous medium. The complexes' emission is quenched by TNP due to a specific O-H···O interaction between the TNP and the ancillary ligand of the complexes, which results in the liberation of the Hoz unit. This explains the high selectivity for TNP and is a conceptually different mechanism compared with previous nitro-aromatic sensors. The combined selectivity and sensitivity of complexes **1-4** (especially **1**) means they strongly compete with other luminescent materials[6,22,24] as viable sensors for detecting TNP. In addition, a test paper demonstrated the naked-eye detection of trace amounts of TNP.

The work was funded by NSFC (No.51473028), the key scientific and technological project of Jilin province (20150204011GX, 20160307016GX), the development and reform commission of Jilin province (20160058). Work in Durham was funded by EPSRC grant EP/L02621X/1.

Conflicts of interest

There are no conflicts to declare.

Notes and references

[a] Key Laboratory of Nanobiosensing and Nanobioanalysis at Universities of Jilin Province, Department of Chemistry, Northeast Normal University, 5268 Renmin Street, Changchun, Jilin Province 130024, P. R. China.
E-mail: zhudx047@nenu.edu.cn, zmsu@nenu.edu.cn
[b] Department of Chemistry, Durham University, Durham, DH1 3LE, UK. E-mail: m.r.bryce@durham.ac.uk

† Electronic supplementary information (ESI) available: Experimental details, ^{1}H NMR spectra, ^{19}F NMR spectra, mass spectra, absorption and emission spectra and procedures for the DFT calculations. CCDC 1573144, 1573145, 1573146, 1573147 and 1573148. For ESI and crystallographic data in CIF or other electronic format see DOI: 10.1039/c000000x/

1 (a) M. E. Germain and M. J. Knapp, *Chem. Soc. Rev.*, 2009, **38**, 2543; (b) Y. Salinas, R. M. -Máñez, M. D. Marcos, F. Sancenón, A. M. Costero, M. Parraad and S. Gil, *Chem. Soc. Rev.*, 2012, **41**, 1261; (c) K. S. Asha, G. S. Vaisakhan and S. Mandal, *Nanoscale*, 2016, **8**, 11782.
2 (a) E. G. Kayser and N. E. Burlinson, *J. Energetic Mater.*, 1988, **6**, 45; (b) J.-F. Xiong, J.-X. Li, G.-Z. Mo, J. -P. Huo, J.-Y. Liu, X.-Y. Chen and Z.-Y. Wang, *J. Org. Chem.*, 2014, **79**, 11619.
3 D. Dinda, A. Gupta, B. K. Shaw, S. Sadhu and S. K. Saha, *ACS Appl. Mater. Interfaces*, 2014, **6**, 10722.
4 T.-P. Huynh, A. Wojnarowicz, A. Kelm, P. Woznicki, P. Borowicz, A. Majka, F. D'Souza and W. Kutner, *ACS. Sens.*, 2016, **1**, 636.
5 (a) S. J. Toal and W. C. Trogler, *J. Mater. Chem.*, 2006, **16**, 2871; (b) I. A. Popov, H. Chen, O. N. Kharybin, E. N. Nikolaev and R. G. Cooks, *Chem. Commun.*, 2005, 1953.
6 (a) Y. Peng, A.-J. Zhang, M. Dong and Y.-W. Wang, *Chem. Commun.*, 2011, **47**, 4505; (b) M. Dong, Y.-W. Wang, A-J. Zhang and Y. Peng, *Chem. Asian J.*, 2013, **8**, 1321; (c) Y. Xu, B. Li, W. Li, J. Zhao, S. Sun and Y. Pang, *Chem. Commun.*, 2013, **49**, 4764; (d) S. Kaur, A. Gupta, V. Bhalla and M. Kumar, *J. Mater. Chem. C*, 2014, **2**, 7356; (e) V. Bhalla, H. Arora, H. Singh and M. Kumar, *Dalton Trans.*, 2013, **42**, 969. (f) M. Kumar, S. I. Reja and V. Bhalla, *Org. Lett.*, 2012, **14**, 6084; (g) D. Li, J. Liu, R. T. K. Kwok, Z. Liang, B. Z. Tang and J. Yu, *Chem. Commun.*, 2012, **48**, 7167; (h) Z-H. Fu, Y-W. Wang and Y. Peng, *Chem. Commun.*, 2017, **53**, 10524.
7 E. R. Goldman, I. L. Medintz, J. L. Whitley, A. Hayhurst, A. R. Clapp, H. T. Uyeda, J. R. Deschamps, M. E. Lassman and H. Mattoussi, *J. Am. Chem. Soc.*, 2005, **127**, 6744.
8 (a) S. Pramanik, C. Zheng, X. Zhang, T. J. Emge and J. L, *J. Am. Chem. Soc.*, 2011, **133**, 4153; (b) S. S. Nagarkar, B. Joarder, A. K. Chaudhari, S. Mukherjee and S. K. Ghosh, *Angew. Chem. Int. Ed.*, 2013, **52**, 2881.
9 (a) M. D. Woodka and V. P. Schnee, *Anal. Chem.*, 2010, **82**, 9917. (b) S. Kazunori and T. M. Swager, *Bull. Chem. Soc. Jpn*., 2007, **80**, 2074
10 G. He, G. Zhang, F. Lü and Y. Fang, *Chem. Mater.*, 2009, **21**, 1494.
11 (a) R. H. Friend, R. W. Gymer, A. B. Holmes, J. H. Burroughes, R. N. Marks, C. Taliani, D. D. C. Bradley, D. A. D. Santos, J. L. B. das, M. L. gdlund and W. R. Salaneck, *Nature*, 1999, **397**, 121; (b) K. -Y. Pu and B. Liu, *Adv. Funct. Mater.*, 2009, **19**, 277.
12 J. Luo, Z. Xie, J. W. Y. Lam, L. Cheng, B. Z. Tang, H. Chen, C. Qiu, H. S. Kwok, X. Zhan, Y. Liu and D. Zhu, *Chem.Commun.*, 2001, 1740.
13 B.-K. An, S.-K. Kwon, S.-D. Jung and S. Y. Park, *J. Am. Chem. Soc.*, 2002, **124**, 14410.
14 (a) M. Yu, Q. Zhao, L. Shi, F. Li, Z. Zhou, H. Yang, T. Yi and C. Huang, *Chem. Commun.*, 2008, 2115; (b) Y. Tao, M. Li, J. Ren and X. Qu, Chem. Soc. Rev., 2015, **44**, 8636; (c) S. Lin, W. Gao, Z. Tian, C. Yang, L. Lu, J.-L. Mergny, C.-H. Leung and D.-L. Ma, *Chem. Sci.*, 2015, **6**, 4284;
15 (a) P. Alam, G. Kaur, C. Climent, S. Pasha, D. Casanova, P. Alemany, A. R. Choudhury and I. R. Laskar, *Dalton. Trans.*, 2014, **43**, 16431; (b) W. Wang, Z. Mao, M. Wang, L. J. Liu, D. W. Kwong, C. H. Leung and D. L. Ma, *Chem. Commun.*, 2016, **52**, 3611.
16 (a) Y. Chi and P. T. Chou, *Chem. Soc. Rev.*, 2010, **39**, 638; (b) Q. Zhao, F. Li and C. Huang, *Chem. Soc. Rev.*, 2010, **39**, 3007; (c) C. Ulbricht, B. Beyer, C. Friebe, A. Winter and U. S. Schubert, *Adv. Mater.*, 2009, **21**, 4418; (d) S. Ladouceur and E. Zysman-Colman, *Eur. J. Inorg. Chem.*, 2013, **17**, 2985.
17 L.-L. Wen, X.-G. Hou, G.-G. Shan, W.-L. Song, S.-R. Zhang, H.-Z. Sun and Z.-M. Su, *J. Mater. Chem. C*, 2017, **5**, 10847.
18 (a) G. Li, W. Guan, S. Du, D. Zhu, G. Shan, X. Zhu, L. Yan, Z. Su, M. R. Bryce and A. P. Monkman, *Chem. Commun.*, 2015, **51**, 16924; (b) Z. Mao, M. Wang, J. Liu, L. J. Liu, S. M. Lee, C. H. Leung and D. L. Ma, *Chem. Commun.*, 2016, **52**, 4450; (c) Y. Han, H.-T. Cao, H.-Z. Sun, G.-G. Shan, Y. Wu, Z.-M. Su and Y. Liao, *J. Mater. Chem. C.*, 2015, **3**, 2341.
19 (a) J. Zhou, Z. Chang, Y. Jiang, B. He, M. Du, P. Lu, Y. Hong, H. S. Kwok, A. Qin, H. Qiu, Z. Zhao and B. Z. Tang, *Chem. Commun.*, 2013, **49**, 2491; (b) Y. Hong, J. W. Y. Lam and B. Z. Tang, *Chem. Soc. Rev.*, 2011, **40**, 5361; (c) G. Li, Y. Wu, G. Shan, W. Che, D. Zhu, B. Song, L. Yan, Z. Su and M. R. Bryce, *Chem. Commun.*, 2014, **50**, 6977.
20 K. Chao, K. Shao, T. Peng, D. Zhu, Y. Wang, Y. Liu, Z. Su and M. R. Bryce, *J. Mater. Chem. C*, 2013, **1**, 6800.
21(a) X.-G. Hou, Y. Wu, H.-T. Cao, H.-Z. Sun, H.-B. Li, G.-G. Shan and Z.-M. Su, *Chem. Commun.*, 2014, **50**, 6031; (b) K. S. Bejoymohandas, T. M. George, S. Bhattacharya, S. Natarajan and M. L. P. Reddy, *J. Mater. Chem. C*, 2014, **2**, 515; (c) T. Fei, K. Jiang and T. Zhang, *Sensors Actuators B*, 2014, **199**, 148.
22 P. Alam, G. Kaur, V. Kachwal, A. Gupta, A. R. Choudhury and I. R. Laskar, *J. Mater. Chem. C*, 2015, **3**, 5450.
23 S. S. Nagarkar, A. V. Desai and S. K. Ghosh, *CrystEngComm.*, 2016, **18**, 2994.
24 B. Gole, A. K. Bar and P. S. Mukherjee, *Chem. Eur. J.*, 2014, **20**, 13321.
25 Y. Cui, L.-L. Wen, G.-G. Shan, H.-Z. Sun, H.-T. Mao, M. Zhang and Z.-M. Su, *Sensors Actuators B*, 2017, **244**, 314.
26 J. Xu, Y. Zhang, H. Yu, X. Gao and S. Shao, *Anal. Chem.*, 2016, **88**, 1455.
27 N. Dey, S. K. Samanta and S. Bhattacharya, *ACS Appl. Mater. Interfaces*, 2013, **5**, 8394.

Supporting Information

Selective sensing of 2,4,6-trinitrophenol (TNP) in aqueous media with "aggregation-induced emission enhancement" (AIEE)-active iridium(III) complexes

Weilong Che,[a] Guangfu Li,[a] Xingman Liu,[a] Kuizhan Shao,[a] Dongxia Zhu,*[a] Zhongmin Su*[a] and Martin R. Bryce*[b]

[a] Key Laboratory of Nanobiosensing and Nanobioanalysis at Universities of Jilin Province, Department of Chemistry, Northeast Normal University, 5268 Renmin Street, Changchun, Jilin Province 130024, P.R. China E-mail: zhudx047@nenu.edu.cn, zmsu@nenu.edu.cn

[b] Department of Chemistry, Durham University, Durham, DH1 3LE, UK
E-mail: m.r.bryce@durham.ac.uk

Table of Contents

1. Experimental - general information

Materials obtained from commercial suppliers were used without further purification unless otherwise stated. All glassware, syringes, magnetic stirring bars, and needles were thoroughly dried in a convection oven. Reactions were monitored using thin layer chromatography (TLC).

Commercial TLC plates were used and the spots were visualised under UV light at 254 and 365 nm. ^{1}H NMR spectra were recorded at 25 ºC on a Varian 500 MHz spectrometer. The chemical shifts (δ) are given in parts per million relative to internal standard TMS. The ^{1}H NMR spectra were referenced internally to the residual proton resonance in DMSO-d_6 (δ 2.49 ppm). The molecular weights of the complexes were obtained by using matrix-assisted laser desorption-ionization time-of-flight (MALDI-TOF) mass spectrometry. Elemental analysis was obtained using a Flash EA1112 analyser. UV-vis absorption spectra were recorded on a Shimadzu UV-3100 spectrophotometer. Photoluminescence spectra were collected on a Shimadzu RF-5301pc spectrophotometer and a Maya 2000Pro optical fiber spectrophotometer. PL efficiencies were measured with an integrating sphere (C-701, Labsphere Inc.) with a 365 nm Ocean Optics LLS-LED as the excitation source, and the laser was introduced into the sphere through the optical fiber.

2. Complexes 1-4 - synthesis and characterization

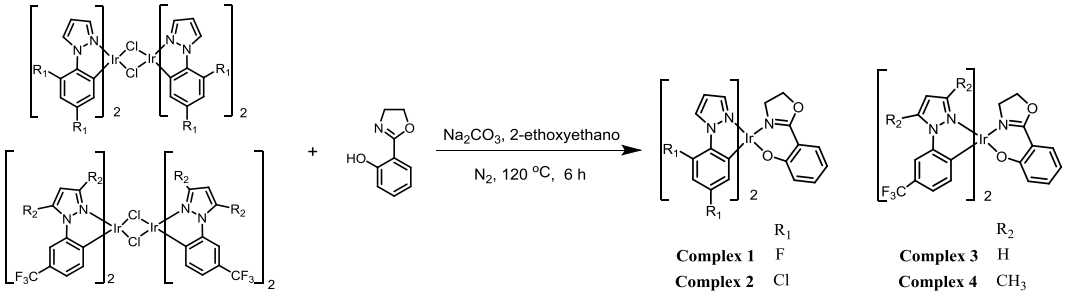

Scheme S1 Synthetic route to complexes **1-4**.

Synthesis of [(1-(2,4-difluorophenyl)-1H-pyrazole)$_2$Ir(oz)] (complex 1)

A procedure in the literature was applied for the synthesis of Hoz.[1] The complex [(1-(2,4-difluorophenyl)-1H-pyrazole)$_2$Ir(μ-Cl)]$_2$ was synthesized by the standard procedure.[2] A mixture of [(1-(2,4-difluorophenyl)-1H-pyrazole)$_2$Ir(μ-Cl)]$_2$ (0.375 g, 0.330 mmol), Na_2CO_3 (0.349 g, 3.20 mmol), and Hoz (0.114 g, 0.70 mmol) dissolved in 2-ethoxyethanol (30 mL) was stirred under an N_2 atmosphere at 130 ºC for 6 h. EtOAc (150 mL) was added after the solution was cooled to RT and washed with water (100 mL) to remove 2-ethoxyethanol. The precipitate was collected by filtration and washed with ethanol (20 mL), followed by diethyl ether (10 mL). Silica gel column purification with n-hexane: EtOAc (5:1 v/v) as eluent gave complex **1** as a green powder (0.329 g, 70% yield). ^{1}H NMR (DMSO-d_6, 500 MHz, δ [ppm]) δ 8.58 (d, J = 5 Hz, 2H), 8.03 (d, J = 3 Hz, 1H), 7.53 (d, J = 5 Hz, 1H), 7.50 (d, J = 2 Hz, 1H), 7.10 (t, J = 6 Hz, 1H) 6.84-6.89 (m, 4H), 6.51 (d, J = 8 Hz, 1H), 6.33 (t, J = 10 Hz, 1H), 5.63 (d, J = 5 Hz, 1H), 5.51 (d, J = 7.5 Hz, 1H), 4.44-4.49 (m, 1H), 4.28-4.33 (m, 1H), 3.71-3.76 (m, 1H), 2.98-3.03 (m, 1H). MS: m/z = 713.10 (M^+). Anal. calcd for $C_{27}H_{18}F_4IrN_5O_2$: C 45.50, H 2.55, N 9.83; found: C 45.62, H 2.73, N 9.64. Crystals for X-ray analysis were obtained by slow evaporation of a dichloromethane-methanol solution of the complex.

Synthesis of [(1-(2,4-dichlorophenyl)-1H-pyrazole)$_2$Ir(oz)] (complex 2)

The synthesis of complex **2** was similar to that of complex **1** except that the cyclometalated ligand used for **2** was 1-(2,4-dichlorophenyl)-1H-pyrazole. Complex **2** was obtained as a yellowish-green solid (0.374 g, 73% yield). ^{1}H NMR (DMSO-d_6, 500 MHz, δ [ppm]) δ 9.21 (t,

J = 7.5 Hz, 2H), 8.11 (d, *J* = 2. Hz, 1H), 7.58 (d, *J* = 2. Hz, 1H), 7.52 (d, *J* = 5 Hz, 1H), 7.17 (d, *J* = 2.5 Hz, 1H), 7.14 (d, *J* = 2 Hz, 1H), 7.09 (t, *J* = 5 Hz, 1H), 6.92 (s, 2H), 6.50 (d, *J* = 7 Hz, 1H), 6.33 (t, *J* = 6 Hz, 1H), 5.95 (d, *J* = 2 Hz, 1H), 5.81 (d, *J* = 2.5 Hz, 1H), 4.43-4.48 (m, 1H), 4.28-4.33 (m, 1H), 3.67-3.72 (m, 1H), 2.93-2.98 (m, 1H). MS: m/z = 776.98 (M^+). Anal. calcd for $C_{27}H_{18}Cl_4IrN_5O_2$: C 41.66, H 2.33, N 9.00; found: C 41.83, H 2.27, N 9.04.

Synthesis of [(1-(3-(trifluoromethyl)phenyl)-1H-pyrazole)$_2$Ir(oz)] (complex 3)

The synthesis of complex **3** was similar to that of complex **1** except that the cyclometalated ligand used for **3** was 1-(3-(trifluoromethyl)phenyl)-1H-pyrazole. Complex **3** was obtained as a green solid (0.338 g, 66% yield). ^{1}H NMR (DMSO-d_6, 500 MHz, δ [ppm]) δ 9.04 (t, *J* = 5 Hz, 2H), 8.00 (d, *J* = 2.5 Hz, 1H), 7.97 (s, 2H), 7.52 (d, *J* = 7.5 Hz, 1H), 7.48 (d, *J* = 3 Hz, 1H), 7.07 (t, *J* = 7.5 Hz, 1H), 6.94 (t, *J* = 7.5 Hz, 2H), 6.84-6.86 (m, 2H), 6.47 (d, *J* = 10 Hz, 1H), 6.36 (d, *J* = 6.5 Hz, 1H), 6.30 (t, *J* = 6 Hz, 1H), 6.25 (d, *J* = 7 Hz, 1H), 4.40-4.45 (m, 1H), 4.25-4.29 (m, 1H), 3.67-3.70 (m, 1H), 2.92-2.95 (m, 1H). MS: m/z = 777.12 (M^+). Anal. calcd for $C_{29}H_{20}F_6IrN_5O_2$: C 44.84, H 2.60, N 9.02; found: C 44.96, H 2.52, N 6.21.

Synthesis of [(3,5-dimethyl-1-(3-(trifluoromethyl)phenyl)-1H-pyrazole)$_2$Ir(oz)] (complex 4)

The synthesis of complex **4** was similar to that of complex **1** except that the cyclometalated ligand used for **4** was 3,5-dimethyl-1-(3-(trifluoromethyl)phenyl)-1H-pyrazole. Complex **4** was obtained as a yellowish-green solid (0.379 g, 69% yield). ^{1}H NMR (DMSO-d_6, 500 MHz, δ [ppm]) δ 7.54 (t, *J* = 10 Hz, 3H), 7.03 (t, *J* = 6 Hz, 1H), 6.93 (d, *J* = 7.5 Hz, 2H), 6.48 (s, 1H), 6.43 (d, *J* = 7 Hz, 1H), 6.41 (s, 1H), 6.37 (d, *J* = 7 Hz, 1H), 6.32 (d, *J* = 6.5 Hz, 1H), 6.26 (t, *J* = 6 Hz, 1H), 4.26-4.30 (m, 1H), 4.21-4.25 (m, 1H), 3.41-3.45 (m, 1H), 2.91-2.95 (m, 1H), 2.89 (s, 3H), 2.87 (s, 3H), 2.27 (s, 3H), 2.21 (s, 3H). MS: m/z = 833.18 (M^+). Anal. calcd for $C_{33}H_{28}F_6IrN_5O_2$: C 47.59, H 3.39, N 8.41; found: C 47.71, H 3.32, N 8.33.

3. X-ray crystallographic data

The single crystals of complexes **1-4**, and complex **1**·**TNP**, were obtained by slow evaporation of the compounds dissolved on a dichloromethane-methanol (3:1 v/v) solution (for **1-4**) and a dichloromethane solution (for **1**·**TNP**). For crystal growth of **1**·**TNP**, **1** and **TNP** were mixed in a 1:1 molar ratio. Diffraction data were collected on a Bruker SMART Apex CCD diffractometer using k(Mo-K) radiation (k = 0.71073 Å). Cell refinement and data reduction were made by the SAINT program. The structures were determined using the SHELXTL/PC program. All non-hydrogen atoms were refined anisotropically, whereas hydrogen atoms were placed at the calculated positions and included in the final stage of refinements with fixed parameters. Fig. 3, Fig. S6-S8 and Fig. 7 show Oak Ridge thermal ellipsoid plot (ORTEP) drawings of complexes **1-4** and complex **1**·**TNP**, and crystallographic data for them have been deposited with the Cambridge Crystallographic Data Centre with CCDC deposition number 1573144, 1573145, 1573146, 1573147 and 1573148. These data can be obtained free of charge from The Cambridge Crystallographic Data Centre via www.ccdc.cam.ac.uk/data_request/cif.

Table S1. Crystal data and structure refinement for complex **1**.

	Complex **1**
Empirical formula	$C_{27}H_{18}F_4IrN_5O_2$
Formula weight	720.66
Temperature (K)	293(2)
Crystal system	Tetragonal
Space group	I4(1)/a
a /Å	27.885(6)
b /Å	27.885
c /Å	12.931(3)
α /°	90.000
β /°	90.000
γ /°	90.000
V/Å^3	10055(3)
Z	16
ρ_{calc} (g/cm^3)	1.904
μ/mm^{-1}	5.379
R_{int}	0.0484
Goodness-of-fit on F^2	1.107
R_1[a], wR_2[b] [I>2σ(I)]	0.0265, 0.0658
R_1, wR_2 (all data)	0.0370, 0.0796

[a] $R_1 = \Sigma||Fo| - |Fc||/\Sigma|Fo|$. [b] $wR_2 = \{ \Sigma[w(Fo^2 - Fc^2)^2]/ \Sigma[w(Fo^2)^2]\}^{1/2}$

Table S2. Crystal data and structure refinement for complex **2**.

	Complex **2**
Empirical formula	$C_{27}H_{18}Cl_4IrN_5O_2$
Formula weight	778.46
Temperature (K)	293(2)
Crystal system	Triclinic
Space group	P-1
a /Å	11.546(16)
b /Å	13.292(19)
c /Å	13.599(19)
α /°	109.302(3)
β /°	110.410(2)
γ /°	103.766(3)
V/Å^3	1692.5(4)
Z	2
ρ_{calc} (g/cm^3)	1.528
μ/mm^{-1}	4.289
R_{int}	0.0416
Goodness-of-fit on F^2	1.041
R_1[a], wR_2[b] [I>2σ(I)]	0.0735, 0.2119

R_1, wR_2 (all data)	0.1148, 0.2491

[a] $R_1 = \Sigma||Fo| - |Fc||/\Sigma|Fo|$. [b] $wR_2 = \{ \Sigma[w(Fo^2 - Fc^2)^2]/ \Sigma[w(Fo^2)^2]\}^{1/2}$

Table S3. Crystal data and structure refinement for complex **3**.

	Complex **3**
Empirical formula	$C_{30}H_{24}F_6IrN_5O_3$
Formula weight	808.74
Temperature (K)	293(2)
Crystal system	Monoclinic
Space group	P2(1)/n
a /Å	13.872(16)
b /Å	10.096(12)
c /Å	22.338(3)
α /°	90.000
β /°	105.767(2)
γ /°	90.000
V/Å^3	3010.8(6)
Z	4
ρ_{calc} (g/cm^3)	1.784
μ/mm^{-1}	4.512
R_{int}	0.0548
Goodness-of-fit on F^2	0.939
R_1[a], wR_2[b] [I>2σ(I)]	0.0405, 0.0897
R_1, wR_2 (all data)	0.0734, 0.1010

[a] $R_1 = \Sigma||Fo| - |Fc||/\Sigma|Fo|$. [b] $wR_2 = \{ \Sigma[w(Fo^2 - Fc^2)^2]/ \Sigma[w(Fo^2)^2]\}^{1/2}$

Table S4. Crystal data and structure refinement for complex **4**.

	Complex **4**
Empirical formula	$C_{33}H_{28}F_6IrN_5O_2$
Formula weight	832.80
Temperature (K)	293(2)
Crystal system	Triclinic
Space group	P-1
a /Å	10.047(8)
b /Å	11.116(8)
c /Å	16.257(13)
α /°	98.712(13)
β /°	104.853(14)
γ /°	98.326(14)
V/Å^3	1702.4(2)
Z	2
ρ_{calc} (g/cm^3)	1.625
μ/mm^{-1}	3.991
R_{int}	0.0227
Goodness-of-fit on F^2	1.037

R_1[a], wR_2[b] [I>2σ(I)]	0.0689, 0.1896
R_1, wR_2 (all data)	0.0896, 0.2085

[a] $R_1 = \Sigma||Fo| - |Fc||/\Sigma|Fo|$. [b] $wR_2 = \{ \Sigma[w(Fo^2 - Fc^2)^2]/ \Sigma[w(Fo^2)^2]\}^{1/2}$

Table S5. Crystal data and structure refinement for complex **1**·**TNP**.

	Complex **1**·**TNP**
Empirical formula	$C_{33}H_{21}F_4IrN_8O_9$
Formula weight	941.78
Temperature (K)	293(2)
Crystal system	Monoclinic
Space group	P2(1)/n
a /Å	17.161(3)
b /Å	9.905(2)
c /Å	23.645(5)
α /°	90.000(3)
β /°	104.930(3)
γ /°	90.000(3)
V/Å^3	3883.6(13)
Z	4
ρ_{calc} (g/cm^3)	1.611
μ/mm^{-1}	3.517
R_{int}	0.0730
Goodness-of-fit on F^2	1.219
R_1[a], wR_2[b] [I>2σ(I)]	0.0481, 0.1390
R_1, wR_2 (all data)	0.0743, 0.1606

[a] $R_1 = \Sigma||Fo| - |Fc||/\Sigma|Fo|$. [b] $wR_2 = \{ \Sigma[w(Fo^2 - Fc^2)^2]/ \Sigma[w(Fo^2)^2]\}^{1/2}$

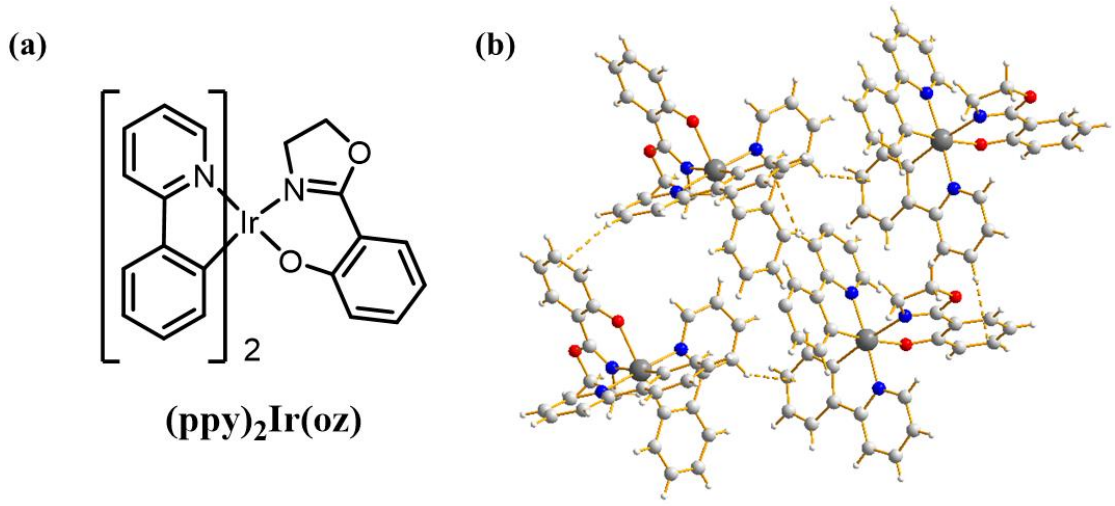

Fig. S1 (a) Chemical structure of $(ppy)_2Ir(oz)$. (b) Molecular packing of $(ppy)_2Ir(oz)$ in the crystal. Data taken from K. Chao, et al, *J. Mater. Chem. C.*, 2013, **1**, 6800. CCDC number 835020.

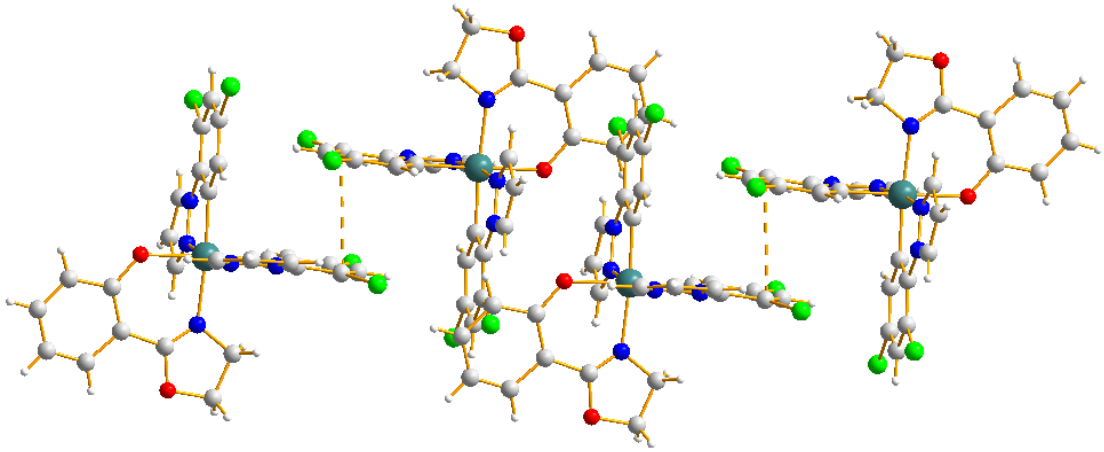

Fig. S2 Molecular packing of complex **2** in the crystal.

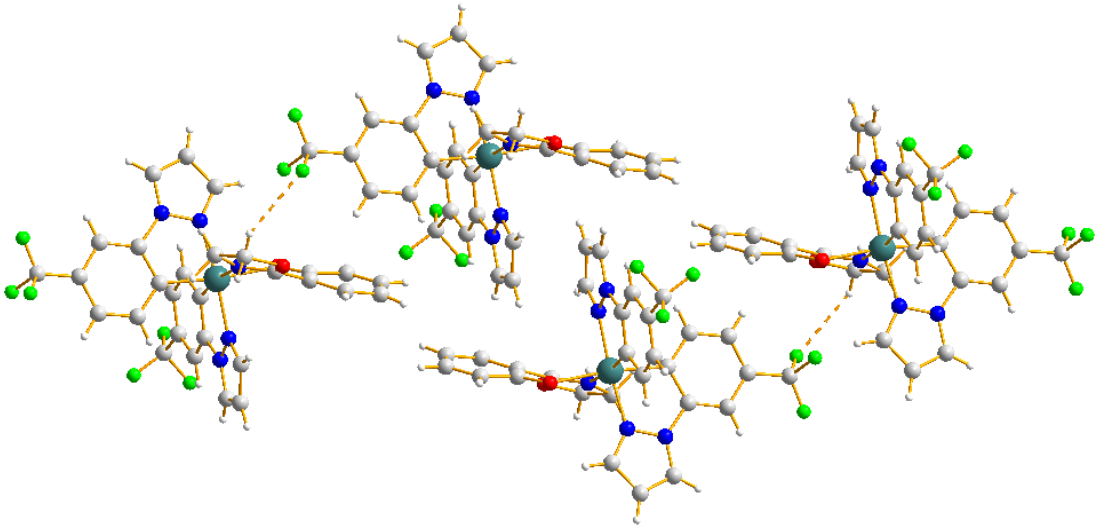

Fig. S3 Molecular packing of complex **3** in the crystal.

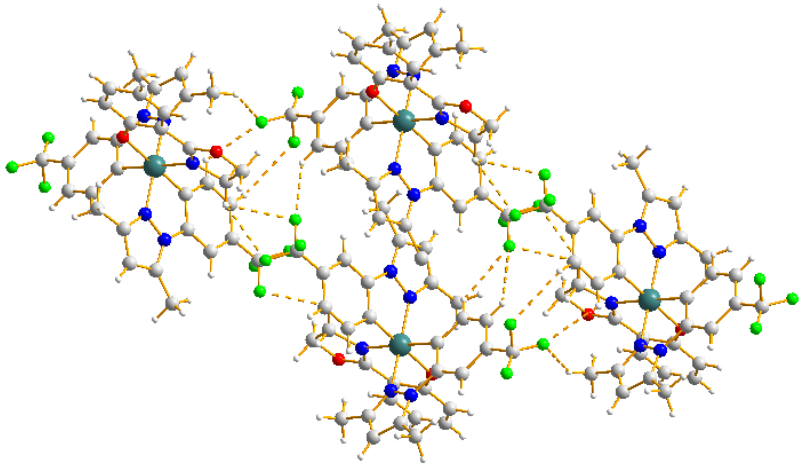

Fig. S4 Molecular packing of complex **4** in the crystal.

4. Photophysical properties

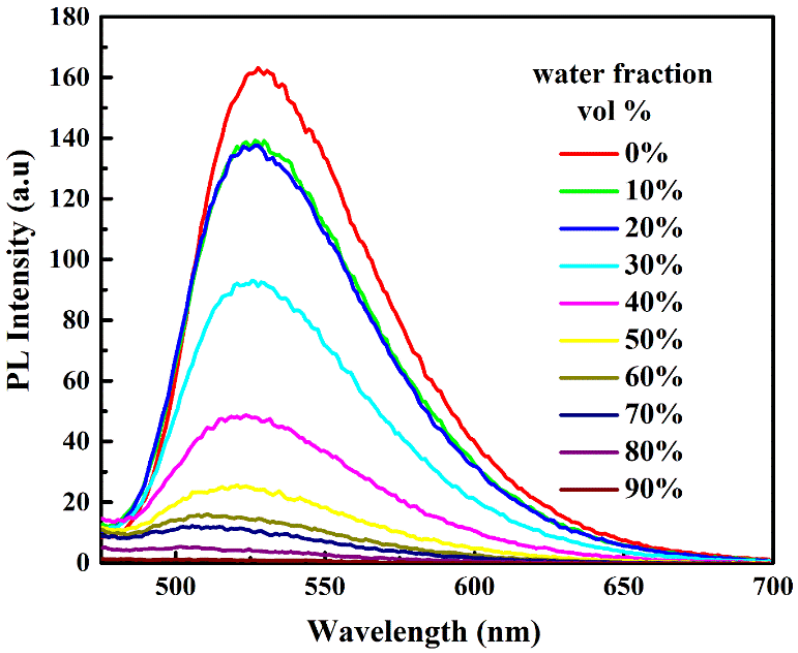

Fig. S5 The PL spectra of $(ppy)_2Ir(oz)$ (10 μM) in acetonitrile-water mixtures with different water fractions at room temperature.

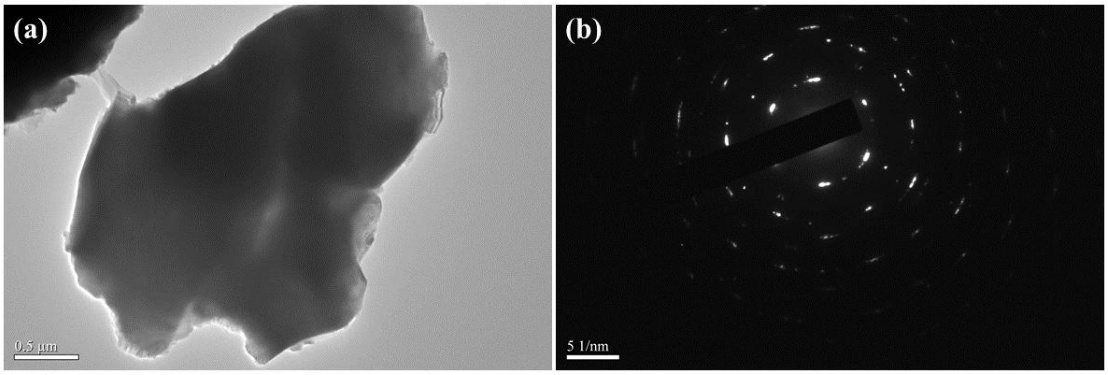

Fig. S6 (a) TEM image of nanoaggregates of complex **1** formed in acetonitrile-water mixtures with 90% water fraction. (b) The electron diffraction pattern of the nanoaggregates.

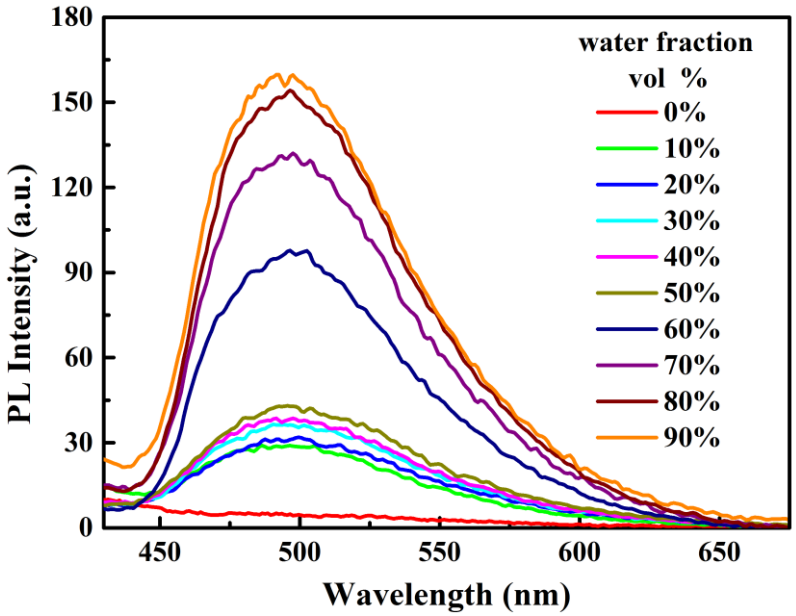

Fig. S7 PL spectra of complex **2** (10 μM) in acetonitrile-water mixtures with different water fractions at room temperature.

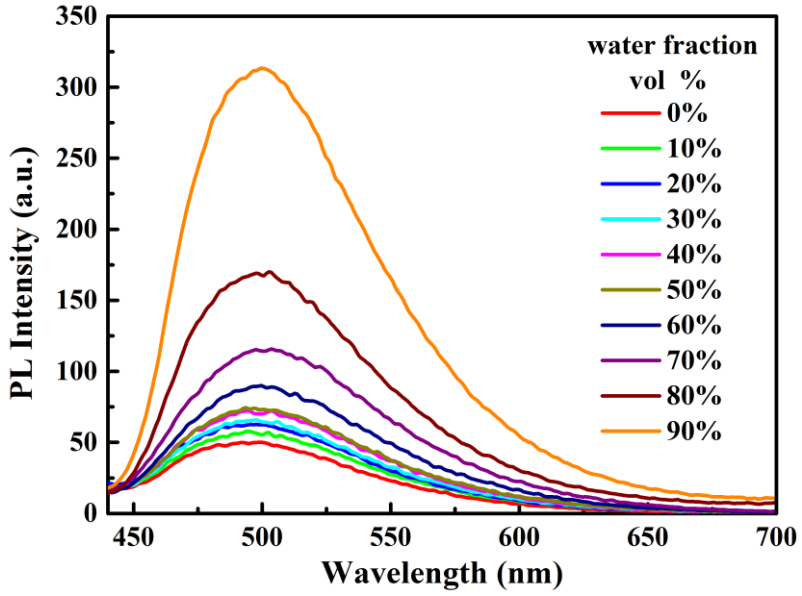

Fig. S8 PL spectra of complex **3** (10 μM) in acetonitrile-water mixtures with different water fractions at room temperature.

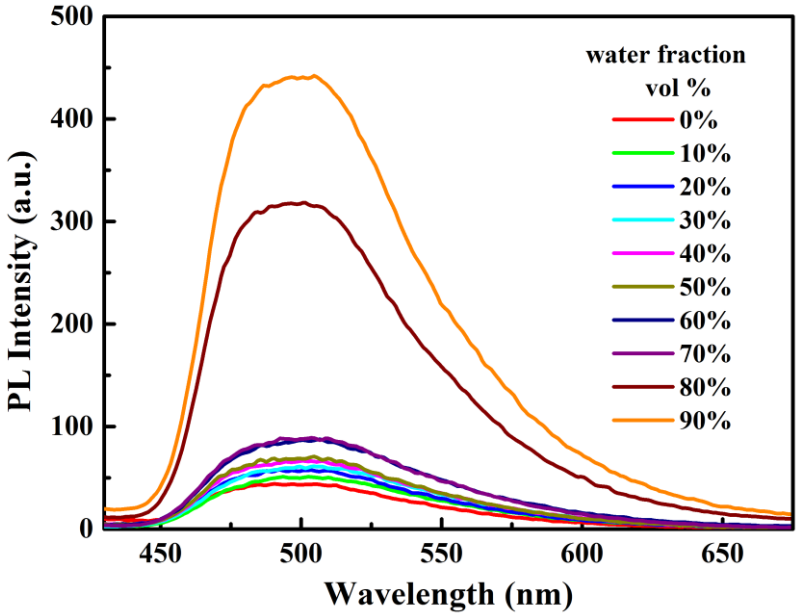

Fig. S9 PL spectra of complex **4** (10 μM) in acetonitrile-water mixtures with different water fractions at room temperature.

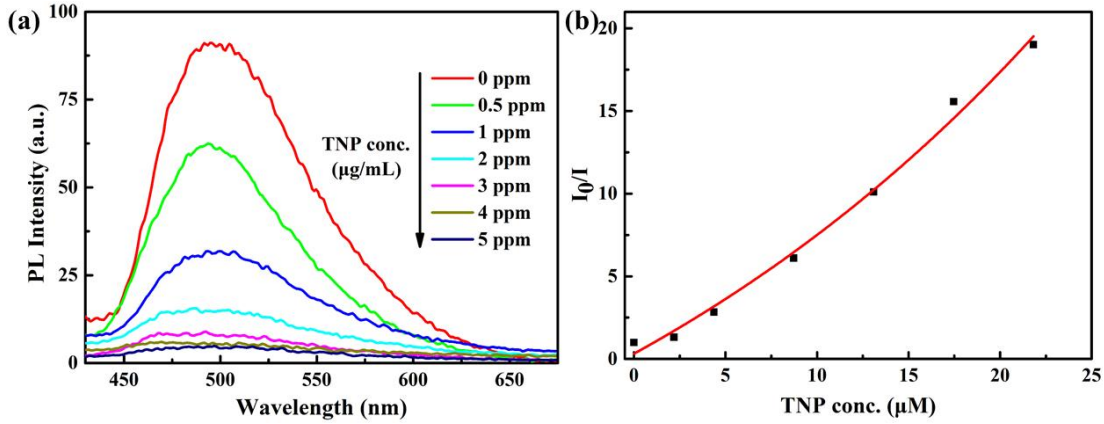

Fig. S10 (a) PL spectra of complex **2** (10 μM) in acetonitrile-water (v/v = 1:9) containing different amounts of TNP. (b) Corresponding Stern-Volmer plot of TNP.

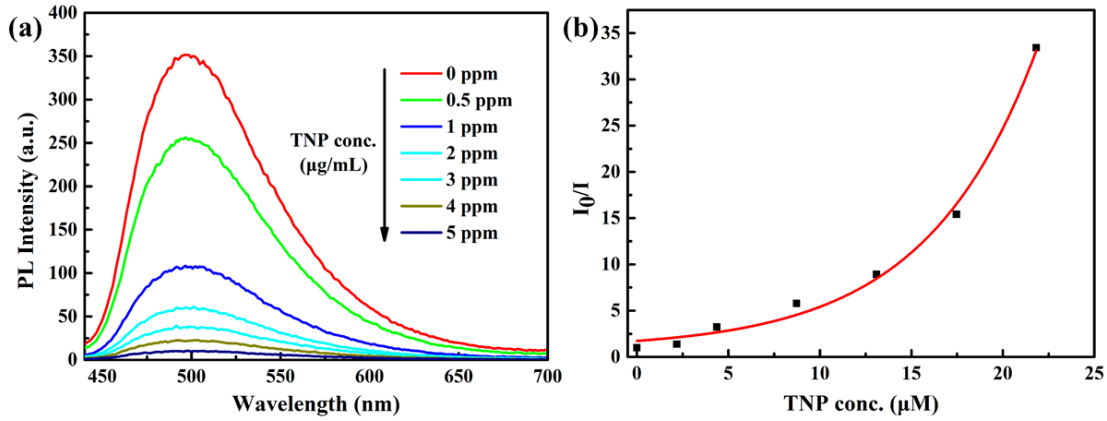

Fig. S11 (a) PL spectra of complex **3** (10 μM) in acetonitrile-water (v/v = 1:9) containing different amounts of TNP. (b) Corresponding Stern-Volmer plot of TNP.

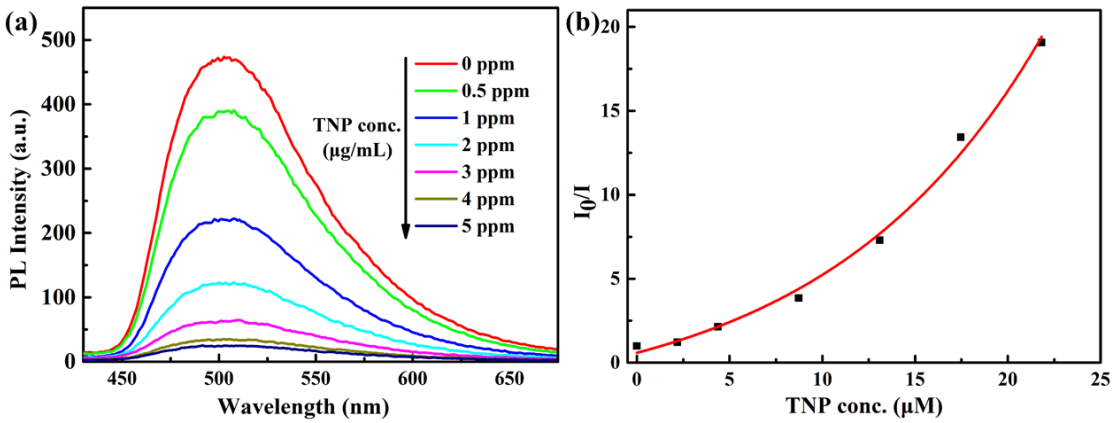

Fig. S12 (a) PL spectra of complex **4** (10 μM) in acetonitrile-water (v/v = 1:9) containing different amounts of TNP. (b) Corresponding Stern-Volmer plot of TNP.

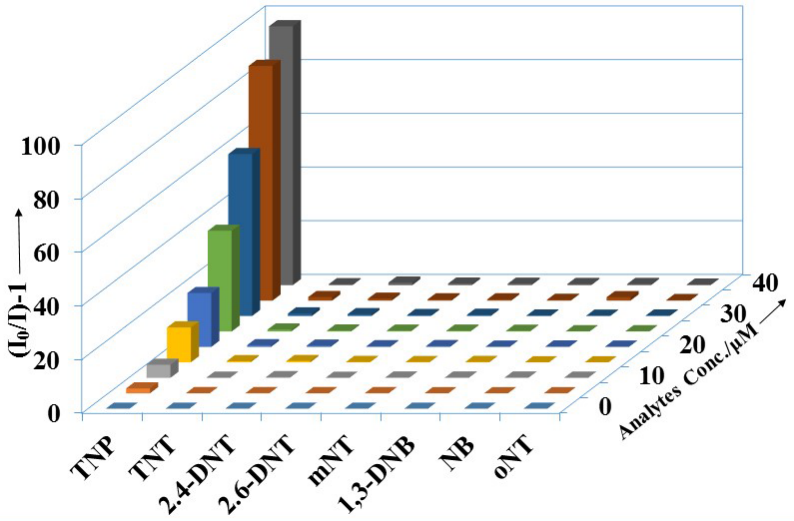

Fig. S13 Stern-Volmer plot of the emission of complex **1** (10 μM) in the presence of different nitro-atomatic compounds in acetonitrile-water (v/v = 1:9) mixtures.

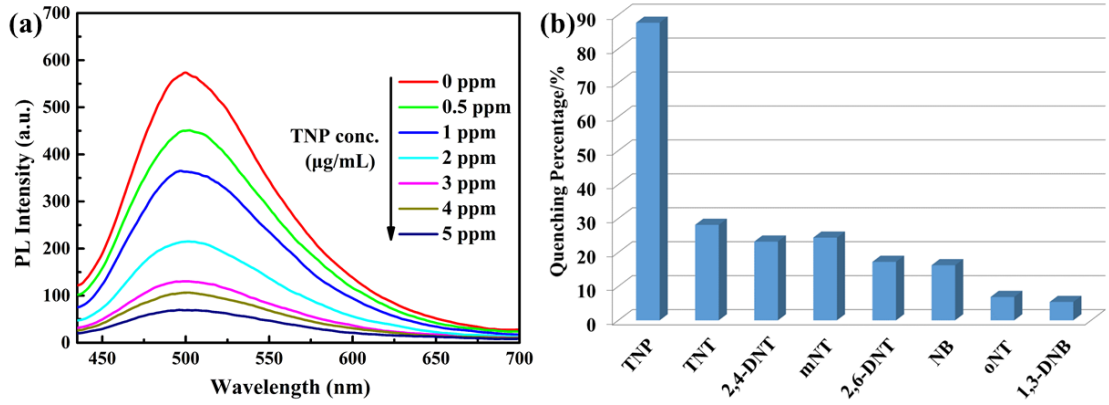

Fig. S14 (a) PL spectra of complex **1** (10 μM) in CH_3CN/aqueous HEPES buffer (1 mM, pH 7.3; 1:4, v/v) solution containing different amounts of TNP. (b) Quenching percentage obtained for different analytes (5 ppm).

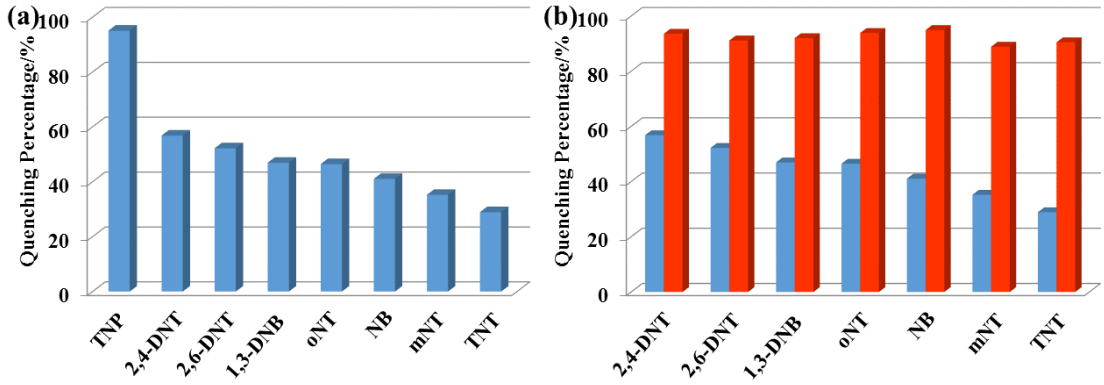

Fig. S15 (a) Quenching percentage obtained for different analytes (5 ppm). (b) Quenching percentage of complex **2** (10 μM) with analytes (5 ppm) in acetonitrile-water (v/v = 1:9) mixtures before (blue) and after (red) the addition of 5 ppm TNP.

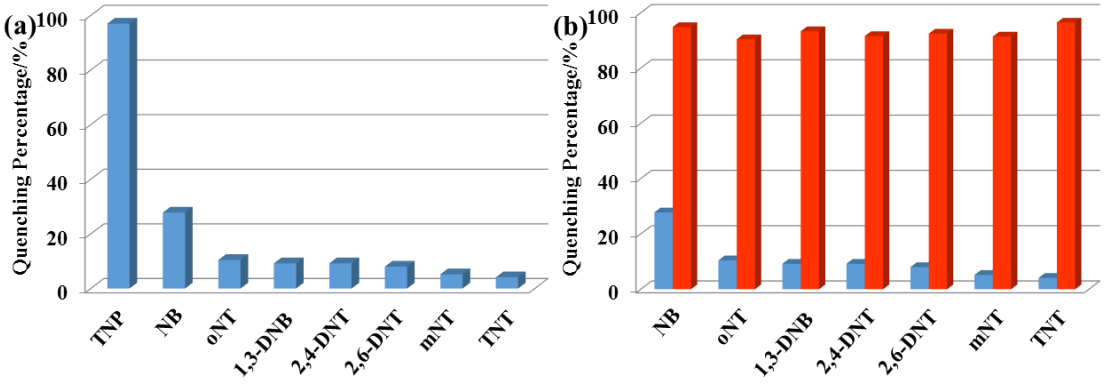

Fig. S16 (a) Quenching percentage obtained for different analytes (5 ppm). (b) Quenching percentage of complex **3** (10 μM) with analytes (5 ppm) in acetonitrile-water (v/v = 1:9) mixtures before (blue) and after (red) the addition of 5 ppm TNP.

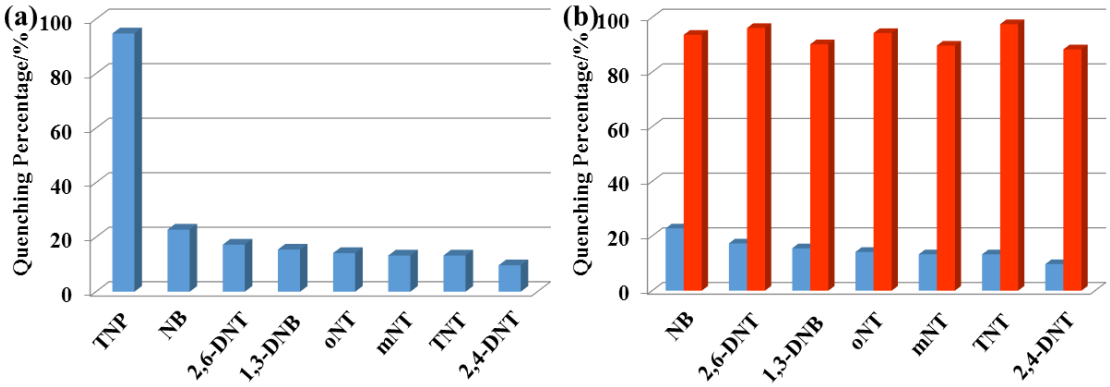

Fig. S17 (a) Quenching percentage obtained for different analytes (5 ppm). (b) Quenching percentage of complex **4** (10 μM) with analytes (5 ppm) in acetonitrile-water (v/v = 1:9) mixtures before (blue) and after (red) the addition of 5 ppm TNP.

Structure-property relationships. The quenching constant of complex **1** is larger than that of complex **2**. The structural difference between complex **1** and complex **2** is the different substituents on the cyclometalated ligands. The more electronegative fluorine atoms in complex **1** can enhance the stability of the Ir-C bond between the cyclometalated ligands and

the metal ion[3] and decrease the stability of the Ir-N (and/or Ir-O) bond between the ancillary ligands and the metal ion according to the *trans* effect.[4] Thus, TNP interacts more easily with the ancillary ligand of complex **1**, resulting in a higher quenching constant. Due to the octahedral structure of this series of complexes, the introduction of methyl groups may increase the steric hindrance and weaken the interaction of O-H···O between TNP and the ancillary ligand of complex **4** compared to **3**, resulting in the smaller quenching constant of complex **4** than that of complex **3**.

5. Mechanistic study

TNP can donate a proton to the ancillary ligand leading to decomplexation of the Hoz unit, as shown for complex **1** in Scheme 1. In support of this mechanism, the mass spectrum shows that complex **1** fragments in solution after the addition of TNP (Fig. S18). The mass spectrum of complex **1** (Fig. S18a) has peaks at m/z 714, 736 and 551 which correspond to [complex **1**+H]$^+$, [complex **1**+Na]$^+$ and the (1-(2,4-difluorophenyl)-1*H*-pyrazole)$_2$Ir$^+$ cation. The peaks at m/z 714 and 736 disappear when TNP is added to the solution and the peak at m/z 551 is retained (Fig. S18b). A new peak corresponding to [Hoz+H]$^+$ at m/z 164 appears, which indicates that the Hoz ligand is liberated. ^{1}H NMR experiments in DMSO-d$_6$ provide complementary information (Fig. S19). Owing to the octahedral structure of complex **1**, the chemical environment of each of the methylene protons (H_a and H_b, H_c and H_d) and two pyrazole protons (H_e and H_f) are different. When complex **1** is mixed with TNP, the protons show an obvious change of chemical shift. H_a and H_b, H_c and H_d, H_e and H_f combine into three peaks, each representing two hydrogens, indicating that their chemical environments become the same. These data suggest that the octahedral structure of complex **1** is disrupted by the addition of TNP. ^{19}F NMR analysis of the mixture of complex **1** and TNP further supports these data (Fig. S20). 1-iodo-3-(trifluoromethyl)benzene was added as an internal standard. The four different chemical environments for the fluorine atoms in the octahedral structure of complex **1**, give rise to four peaks in the ^{19}F NMR spectrum. The addition of TNP leads to only two peaks in the ^{19}F NMR spectrum due to two different of chemical environments of the fluorine atoms. These results are entirely consistent with the mechanism in Scheme 1. The mechanism of TNP detection by complexes **2-4** is the same as for complex **1** (Fig. S21-S26).

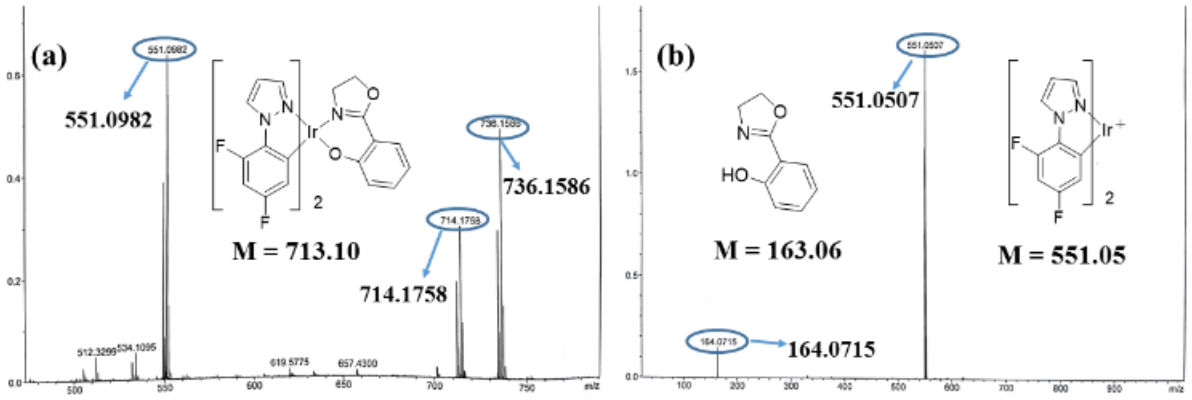

Fig. S18 Mass spectrum of complex **1** (a) before and (b) after addition of 1 equivalent of TNP.

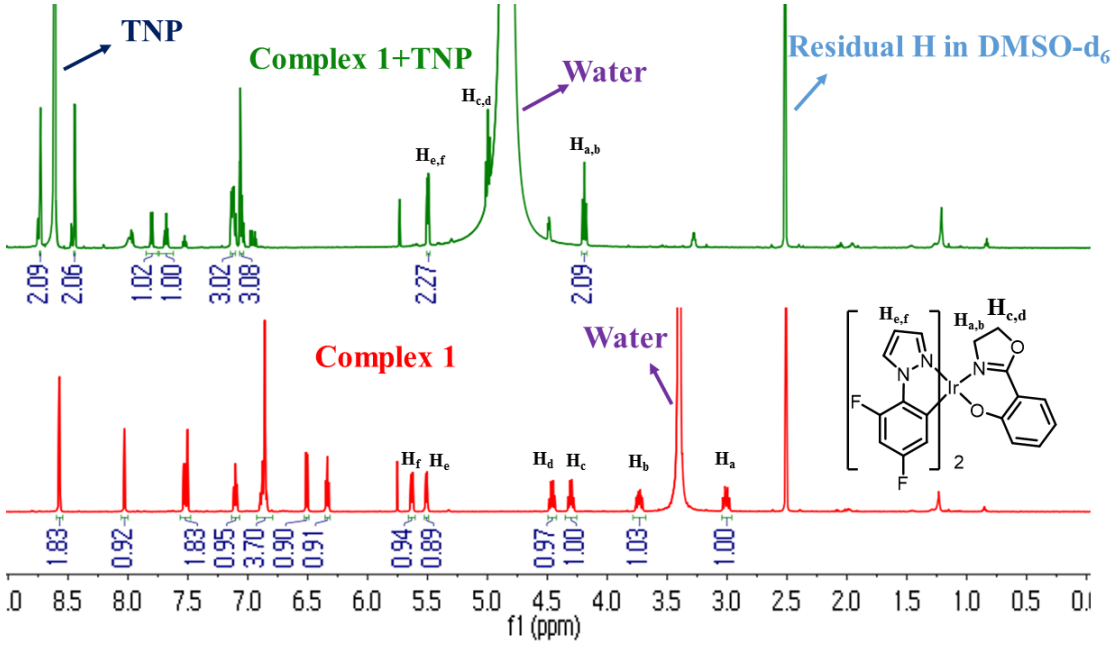

Fig. S19 ^{1}H NMR spectra of complex **1** before and after addition of 1 equivalent of TNP in DMSO-d_6.

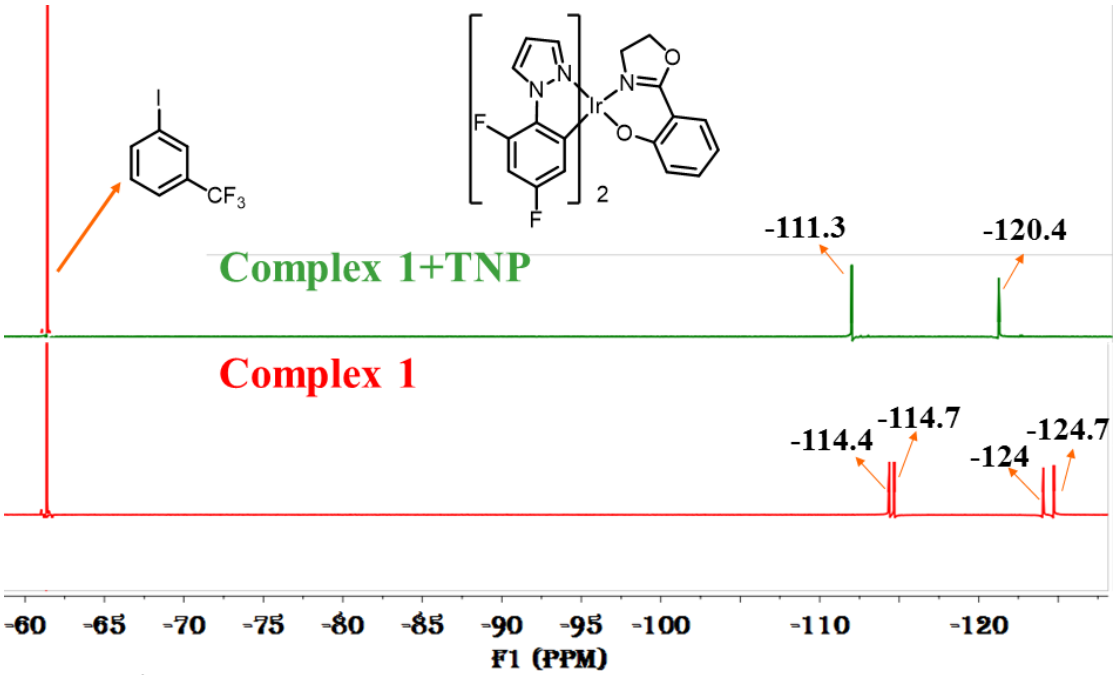

Fig. S20 ^{19}F NMR spectra of complex **1** before and after addition of 1 equivalent of TNP in DMSO-d_6 (internal standard = 1-iodo-3-(trifluoromethyl)benzene).

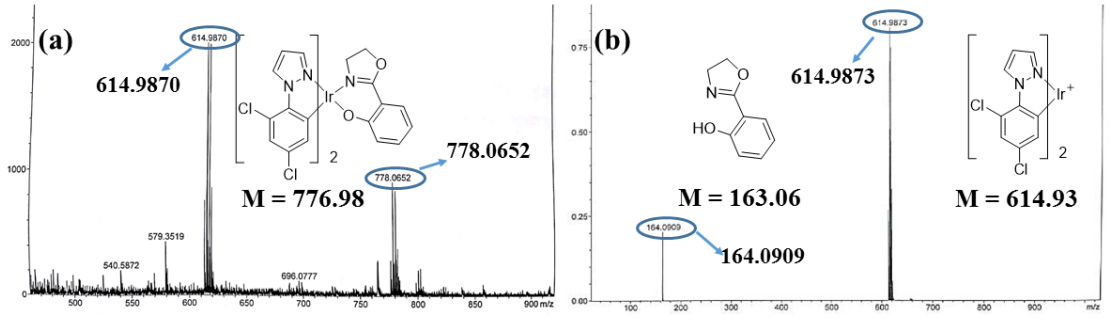

Fig. S21 Mass spectrum of complex **2** (a) before and (b) after addition of 1 equivalent of TNP.

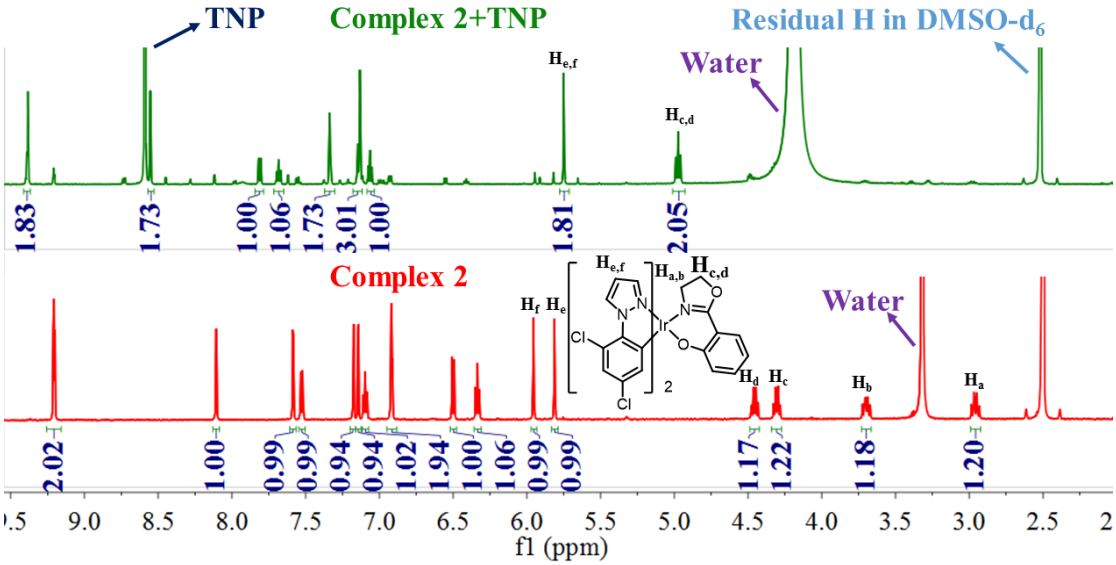

Fig. S22 ^{1}H NMR spectra of complex **2** before and after addition of 1 equivalent of TNP in DMSO-d_6. The H_a and H_b in complex **2**+TNP are contained in the peak of water.

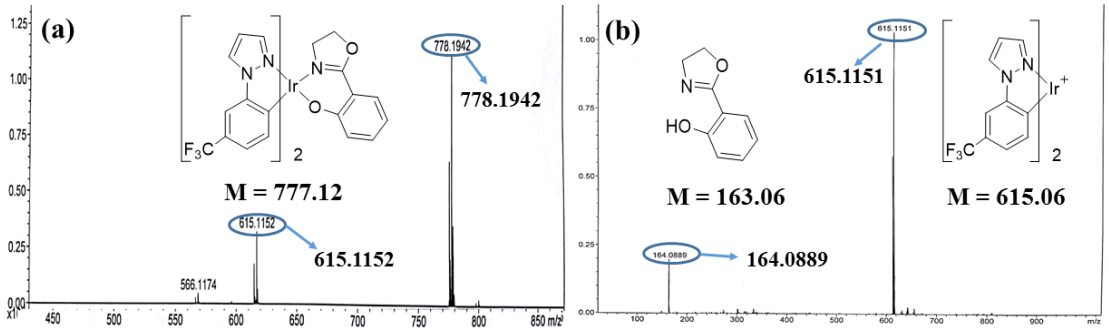

Fig. S23 Mass spectrum of complex **3** (a) before and (b) after addition of 1 equivalent of TNP.

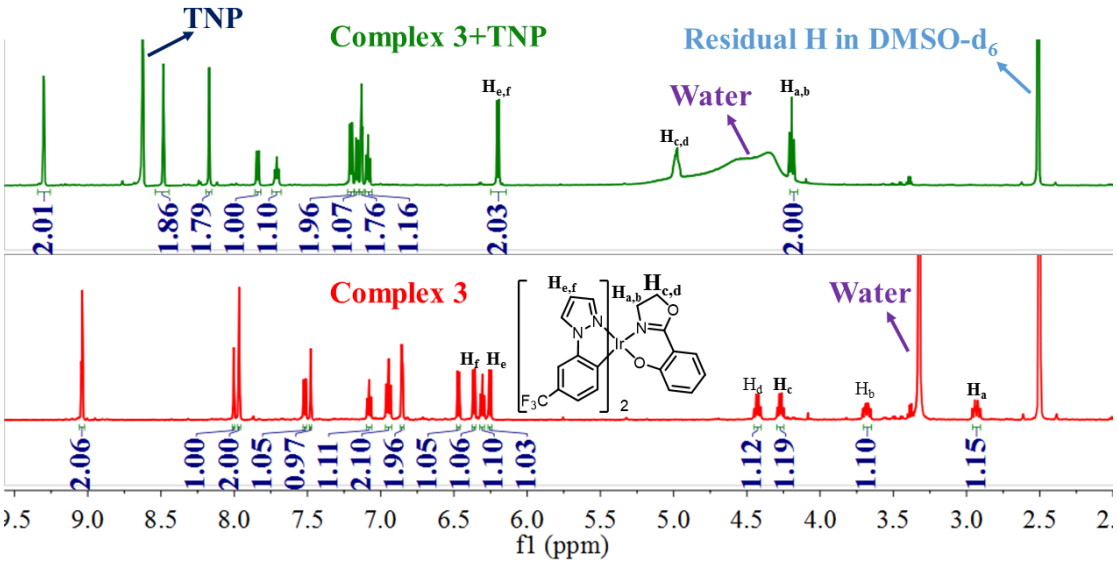

Fig. S24 ^{1}H NMR spectra of complex **3** before and after addition of 1 equivalent of TNP in DMSO-d_6.

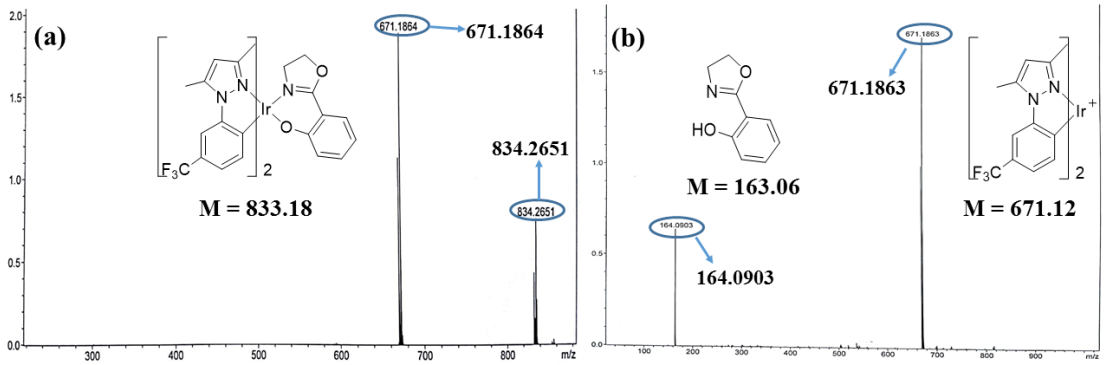

Fig. S25 Mass spectrum of complex **4** (a) before and (b) after addition of 1 equivalent of TNP.

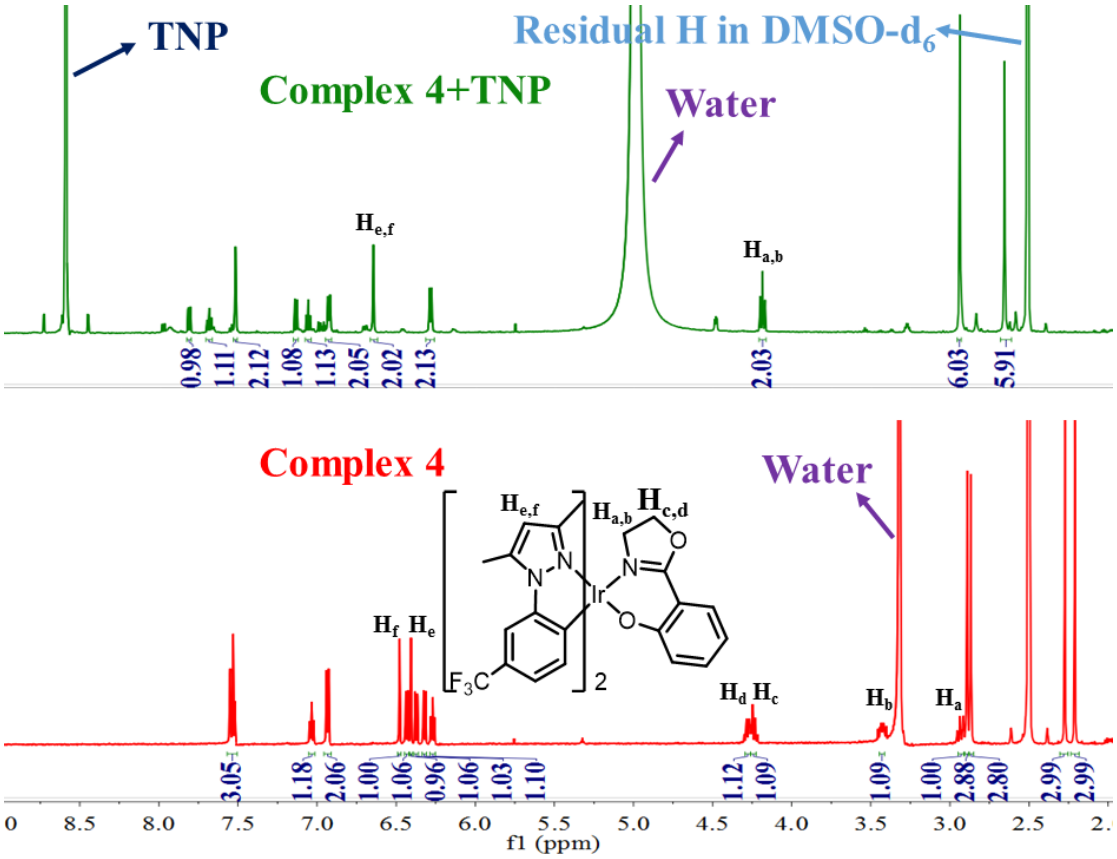

Fig. S26 ^{1}H NMR spectra of complex **4** before and after addition of 1 equivalent of TNP in DMSO-d_6. The H_c and H_d in complex **4**+TNP are contained in the peak of water.

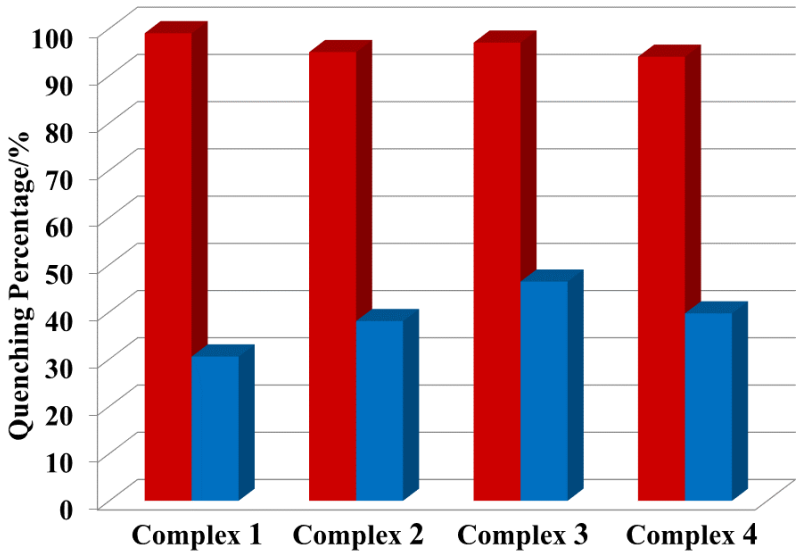

Fig. S27 Quenching percentage of complexes **1-4** (10 μM) with 5 ppm of TNP (red) and 2,4-DNP (blue) in acetonitrile-water (v/v = 1:9).

6. Theoretical calculations

To gain a better understanding of the experimental results, theoretical calculations were performed with Gaussian 09 program.[5] The geometry optimizations were performed by B3LYP methods. The B3LYP functional was employed for all DFT calculations. The 6-31G*

basis set was employed for C, H, N, O, F, Cl atoms, while the iridium atom was described by the Hay-Wadt effective core potential (ECP) and a double-ξ basis set LANL2DZ. The highest occupied molecular orbital (HOMO) and lowest unoccupied molecular orbital (LUMO) energy levels based on the optimized ground-state geometries were calculated (Fig. S27).

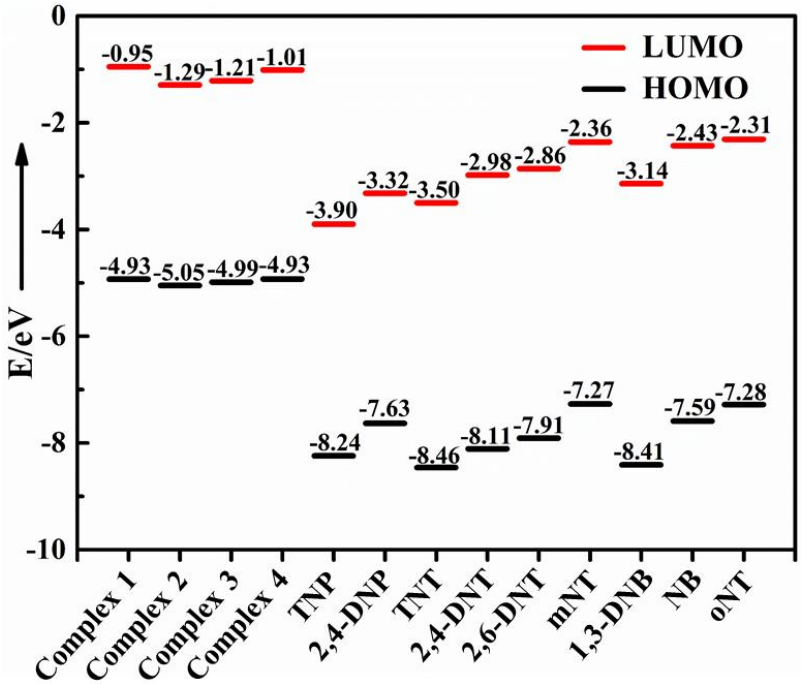

Fig. S28 Calculated HOMO and LUMO energies of complexes **1-4** and the nitro-aromatic explosives.

7. References

1. W. L. Che, T. C. Yu, D. Jin, X. Y. Ren, D. X. Zhu, Z. M. Su and M. R. Bryce, *Inorg. Chem. Commun.*, 2016, **69**, 89.
2. (a) G. G. Shan, H. B. Li, Z. C. Mu, D. X. Zhu, Z. M. Su and Y. Liao, *J. Organomet. Chem.*, 2012, **702**, 27; (b) E. Baranoff, H. J. Bolink, E. C. Constable, M. Delgado, D. Häussinger, C. E. Housecroft, M. K. Nazeeruddin, M. Neuburger, E. Ortí, G. E. Schneider, D. Tordera, R. M. Walliser and J. A. Zampese, *Dalton Trans.*, 2013, **42**, 1073.
3. J. A. Garg, O. Blacque, T. Fox and K. Venkatesan, *Inorg. Chem.*, 2010, **49**, 11463.
4. J. V. Quagliano and L. Schubert, *Chem. Rev.*, 1952, **50**, 201.
5. M. J. Frisch, G. W. Trucks, H. B. Schlegel, G. E. Scuseria, M. A. Robb, J. R. Cheeseman, G. Scalmani, V. Barone, B. Mennucci, G. A. Petersson, H. Nakatsuji, M. Caricato, X. Li, H. P. Hratchian, A. F. Izmaylov, J. Bloino, G. Zheng, J. L. Sonnenberg, M. Hada, M. Ehara, K. Toyota, R. Fukuda, J. Hasegawa, M. Ishida, T. Nakajima, Y. Honda, O. Kitao, H. Nakai, T. Vreven, J. A. Montgomery, Jr., J. E. Peralta, F. Ogliaro, M. Bearpark, J. J. Heyd, E. Brothers, K. N. Kudin, V. N. Staroverov, R. Kobayashi, J. Normand, K. Raghavachari, A. Rendell, J. C. Burant, S. S. Iyengar, J. Tomasi, M. Cossi, N. Rega, J. M. M. Millam, M. Klene, J. E. K. Knox, J. B. C. Cross, V. Bakken, C. Adamo, J. Jaramillo, R. Gomperts, R. E. Stratmann, O. Yazyev, A. J. Austin, R. Cammi, C. Pomelli, J. W. Ochterski, R. L. Martin, K. Morokuma, V. G. Zakrzewski, G. A. Voth, P. Salvador, J. J. Dannenberg, S. Dapprich, A. D. Daniels, O. Farkas, J. B. Foresman, J. V. Ortiz, J. Cioslowski and D. J. Fox, Gaussian 09, Revision A.02, Gaussian, Inc, Wallingford CT, 2009.